Preclinical Evaluation and Pilot Clinical Study of ^{18}F-AlF-labeled FAPI-Tracers for PET Imaging of Cancer Associated Fibroblasts

Kongzhen Hu
Southern Medical University Nanfang Hospital https://orcid.org/0000-0002-7889-9576
Junqi Li
Shenzhen International Institute for BiomedicaIn Research
Lijuan Wang
Southern Medical University Nanfang Hospital
Yong Huang
Chinese Academy of Medical Sciences & Peking Union Medical College
Li Li
Southern Medical University Nanfang Hospital
Shimin Ye
Southern Medical University Nanfang Hospital
Yanjiang Han
Southern Medical University Nanfang Hospital
Shun Huang
Southern Medical University Nanfang Hospital
Hubing Wu
Southern Medical University Nanfang Hospital
Jin Su
Guangzhou Medical College First Affiliated Hospital
Ganghua Tang (gtang0224@smu.edu.cn)
Southern Medical University Nanfang Hospital

Research Article

Keywords: Fibroblast activation protein, 18F-AlF-labeled, PET, Nasopharyngeal cancer, Cancer-associated fibroblasts

Posted Date: March 6th, 2021

DOI: https://doi.org/10.21203/rs.3.rs-265235/v1

Version of Record: A version of this preprint was published at Acta Pharmaceutica Sinica B on October 1st, 2021. See the published version at https://doi.org/10.1016/j.apsb.2021.09.032.

Abstract

Background The recent development of many different types of radiotracers that target the fibroblast activation protein (FAP) has been promising for tumor diagnosis. Here, we set out to develop ^{18}F-labeled FAP tracers for cancer-associated fibroblast imaging and evaluated the potential of these tracers for clinical application.

Methods The non-radioactive reference compounds and labeling precursors were synthesized using organic chemistry and the binding affinities were identified using surface plasmon resonance. Both radioligands (^{18}F-P-FAPI and ^{18}F-FAPI-42) were produced in an automated manner via complexation of Al^{18}F. For *in vitro* characterization of ^{18}F-P-FAPI and ^{18}F-FAPI-42, we conducted studies to determine the partition coefficients, stability, cellular uptake, internalization, and efflux. *In vivo* biodistribution studies and microPET imaging of ^{18}F-P-FAPI and ^{18}F-FAPI-42, in comparison to ^{68}Ga-FAPI-04, were conducted on the A549-FAP tumor bearing mice. Finally, one nasopharyngeal cancer patient underwent whole-body PET/CT after being injected with ^{18}F-P-FAPI.

Results Both ^{18}F-P-FAPI and ^{18}F-FAPI-42 were successful prepared with high specificity, rapid internalization, and potent affinity binding toward FAP. Compared to ^{18}F-FAPI-42, ^{18}F-P-FAPI exhibited lower levels of cellular efflux in the A549-FAP cells and higher stability *in vivo*. Furthermore, *in vivo* studies of ^{18}F-P-FAPI in the A549-FAP tumor model indicated a higher tumor uptake than ^{18}F-FAPI-42 and ^{68}Ga-FAPI-04. An initial diagnostic application in patient with nasopharyngeal cancer, ^{18}F-P-FAPI and ^{18}F-FDG PET/CT showed comparable results for both primary tumors and lymph node metastases.

Conclusion The radiofluorinated FAP-ligands demonstrated promising characteristics in their preclinical evaluation, and the feasibility of cancer-associated fibroblasts imaging was demonstrated using PET studies.

Introduction

Fibroblast activation protein (FAP), a type II transmembrane serine protease, exhibits both post-proline dipeptidyl peptidase and endopeptidase activity [1]. Under physiological conditions, FAP is expressed at little or non-detectable levels in most normal adult tissues, with the exception of multipotent bone marrow stromal cells (BM-MSC) and alpha cells of Langerhans islets [2]. However, FAP is highly upregulated in cancer-associated fibroblasts and in extracellular matrix of the tumor microenvironment [3,4]. It has been proven that FAP levels are related to the survival and prognosis in cancer patients indicating that they have a vital function in cancer development [1,5,6]. Therefore, FAP has become a promising target for cancer diagnosis and treatment. Recently, several PET radiotracers for FAP were successfully developed and imaged *in vivo* [7–11] (Fig. 1). Among these, the ^{68}Ga-labeled ligands have been extensively studied and ^{68}Ga-FAPI-04 has applied in clinical imaging for various types of cancers that have a high tumor-to-noise ratio [7,8,10,12–16]. However, the ^{68}Ga-labeled tracers were limited in the availability of

radionuclide from ^{68}Ge/^{68}Ga-generators and have a relatively short half-life ^{68}Ga ($T_{1/2}$ = 67.7 min, 88.9 % β^+). In contrast, ^{18}F ($T_{1/2}$ = 109.8 min, 96.7 % β^+) is the most widely-utilized radionuclide in PET and can be produced in larger doses by one cyclotron production, and can be delivered over longer distances. Thus far, two ^{18}F-labeled FAP-targeting radiotracers have been developed [9,11]. Haberkor *et al.* reported the use of a ^{18}F-labeled FAP tracer, ^{18}F-FAPI-74, for imaging of lung cancer patients in a clinical setting, but the preclinical data has not been available [9]. Another tracer, ^{18}F-FGlc-FAPI, was reported based on ^{18}F-fluoroglycosylation for FAP imaging by Toms *et al.* [11]. However, the preparation of ^{18}F-FGlc-FAPI with long and laborious multistep syntheses could be limited in a clinical study.

The aim of this study was to develop ^{18}F-FAP tracers through the use of direct labeling via Al^{18}F-chelation. Herein, we present the synthesis and preclinical evaluation of two ^{18}F-labeled FAP ligands ^{18}F-P-FAPI and ^{18}F-FAPI-42. Additionally, we compared the biodistribution and imaging characteristics of synthesized probes with the clinically used FAP tracer ^{68}Ga-FAPI-04 in nude mice xenografts of FAP-positive A549-FAP tumors. Lastly, we selected ^{18}F-P-FAPI and performed pilot studies in patients with cancer.

Materials And Methods

Chemistry

All reagents and solvents were purchased commercially, were of analytical grade and used without further purification. High-resolution mass spectrometry (HRMS) data were acquired using a Thermo Fisher Scientific Orbitrap Fusion mass spectrometer (Thermo Fisher Scientific, San Jose, CA, USA). The synthesis of non-radioactive compounds, which includes reference compounds ^{19}F-P-FAPI and ^{19}F-FAPI-42, and their precursors are described in detail in Supplementary Schemes S1 and S2.

Radiochemistry and Quality Control

No-carrier-added [^{18}F]fluoride was synthesized using an 18 MeV proton bombardment of a high pressure [^{18}O]H_2O target utilizing a General Electric PET trace biomedical cyclotron (PET 800; GE, USA). Sep-Pak Plus QMA and Sep-Pak C18-Light cartridges were purchased from Waters Associates. Radioactivity was quantified through the use of a Capintec CAPRAC-R dose calibrator (NJ, USA).

^{18}F-labeled FAP tracers labeling via Al^{18}F-chelation were produced on a modified AllInOne synthesis module (Trasis, Ans, Belgium), as was previously reported [9,17]. After production in a cyclotron, [^{18}F]F^- were transfer into the module and trapped on a Sep-Pak Plus QMA, which was preconditioned with 5 mL of 0.5 M sodium acetate buffer pH 3.9 and 10 mL of water. Subsequently, [^{18}F]F^- (37~74 GBq) was eluted using 0.35 mL of 0.5 M sodium acetate buffer pH 3.9 to a mixture of $AlCl_3$ (40.0 nmol, 20.0 µL, 2.0 mM in 0.2 M sodium acetate buffer pH 4.0) and precursor (P-FAPI or NOTA-FAPI-42, 80.0 nmol) in 300 µL DMSO. After being heated for 15 min at 105 °C, the mixture was then cooled and diluted with 5 mL of

water. Next, the diluted solution was transferred over an activated C18 cartridge, which was preconditioned with 5 mL ethanol (EtOH) and 10 mL water. Afterwards, the cartridge was washed with 20 mL of water and flushed with nitrogen sequentially. The desired radiolabeled compound was eluted from the C18 cartridge with 1 mL of ethanol/water (1/1, v/v), and the C18 cartridge was flushed using 10 mL of NaCl 0.9%. The eluate was passed through a sterile Millipore filter (0.22 μm) into a sterile vial. The final drug product solution was evaluated quality control, which is described in more detail in Supplementary Method.

Surface Plasmon Resonance (SPR) Binding Assays

The experiments were performed using PlexAray HT (Plexera Bioscience, Seattle, WA, USA). The FAP ligands (10 mM in ddH_2O) were prepared in 384 wells and spotted on 3D photocrosslinked (PCL) chip in a UV-free room with a humidity of 45%. The obtained PCL chips were then dried in a vacuum chamber in order to evaporate the solvent, and the chips were irradiated for 15 min using a 365-nm UV cross-linker instrument (UVJLY-1; Beijing BINTA Instrument Technology Company). The irradiated energy on the surface then amounted to 2.8 J/cm^2. After undergoing UV treatment, the chips were rinsed in *N*,*N*-dimethylformamide (DMSO), EtOH, and ddH_2O for 15 min each. Finally, the chips were dried under nitrogen gas for further use. In order to quantify the interaction between immobilized biomolecules and flowing proteins, an SPR imaging instrument (Kx5; Plexera) was utilized to monitor the whole procedure in real-time. In brief, a chip with well-prepared biomolecular microarrays was assembled using a plastic flow cell for sample loading. The optical architecture and operation details of the PlexArray HT were previously described elsewhere [18]. The protein sample was then prepared at the appropriate concentration in PBS running buffer while a 10 mM glycine-HCl buffer (pH 2.0) was used as a regeneration buffer. A typical binding curve was acquired using a flowing protein sample at 2 μL/s for 300-s association, and then the flowing running buffer for 300-s dissociation, followed by a 200-s regeneration buffer at 3 μL/s. In order to obtain results for binding affinity, seven gradient concentrations of the flowing phase (2000 nM, 1000 nM, 500 nM, 250 nM, 125 nM, 62.5 nM, and 31.3 nM) (protein sample) were prepared and flowed, respectively. All binding signals were converted to standard refractive units (RU) by calibrating every spot with 1% glycerol (wt/vol) in running buffer with a known refractive index change (1,200 RU). Binding data was collected and evaluated using a commercial SPR imaging analysis software (Plexera SPR Data Analysis Model; Plexera).

Partition Coefficient

The *n*-octanol/PBS partition coefficients of ^{18}F-P-FAPI, ^{18}F-FAPI-42, and ^{68}Ga-FAPI-04 were determined, as previously described [19].

Cell lines

Human cell lines A549 (ATCC) was maintained in DMEM (Gibco, USA) supplemented with 10% FBS (Fetal bovine serum, Gibco, USA) and 1% streptomycin and penicillin (Gibco, USA) at 37 °C in 5% CO_2. The

A549-FAP cell line, stably expressed human FAP, was obtained by lentiviral infection, following 2 weeks screening with 2 μg puro (puromycin, Thermo Fisher, USA).

Cell Studies and Animal Models

The detailed protocols for *in vitro* cell studies and animal experiments, including cell uptake, efflux, internalization, and tumor transplantation, are provided in the Supplemental Information File.

In Vitro Stability and *In Vivo* Stability

Detailed procedures for *in vitro* and *in vivo* stability of ^{18}F-P-FAPI and ^{18}F-FAPI-42 are included in the Supplemental Information.

MicroPET Imaging

For dynamic micro-PET imaging studies, either ^{18}F or ^{68}Ga labeled tracer (5.55–11.1 MBq, n = 3) were injected through the lateral tail vein into mice bearing A549-FAP tumors xenograft utilizing an Inveon Micro-PET/CT scanner (Siemens; Erlangen, Germany). Image studies were conducted through the use of a three-dimensional ordered-subset expectation maximum (OSEM) algorithm (Siemens, Erlangen, Germany). For the blocking study, A549-FAP tumor-bearing mice were co-injected using DOTA-FAPI-04 (100 nmol/mouse, n = 3) as competitor. The images and regions of interest (ROIs) were produced through the use of a software, Inevon Research Workplace 4.1 (Siemens, Erlangen, Germany).

Biodistribution Studies

Organ distribution studies were carried out using mice with xenografted A549-FAP tumors with and without DOTA-FAPI-04 (100 nmol/mouse, n = 3). The mice were then injected through the tail vein using ^{18}F-P-FAPI (1.11–1.85 MBq), and were euthanized at 1 h post-injection (p.i.). Organs of interest and tumor were quickly dissected, weighed and radioactivity was quantified through the use of a γ-counter and calculated as percentage of injected dose per gram of tissue (%ID/g).

PET/CT Imaging and Analysis

The PET/CT imaging study was performed on a total-body PET/CT scanner (uEXPLORER, United Imaging Healthcare; Shanghai, China) and granted approval by the Ethics Committee of Nangfang Hospital (No. NFEC-2020-205). These were conducted in accordance with Declaration of Helsinki. The patient signed an informed consent form prior to study participation. A-41-year-old patient with nasopharyngeal cancer was examined using ^{18}F-FDG and ^{18}F-P-FAPI on two consecutive days. The patient received an intravenous injection of ^{18}F-FDG (3.7 MBq/Kg) while fasting for at least 6 h on the first day and ^{18}F-P-FAPI (3.7 MBq/Kg) on the second day without fasting. After 1 h post-injection of ^{18}F-FDG or ^{18}F-P-FAPI, the patient was imaged and PET images were reconstructed through the use of ordered subsets expectation maximization algorithm (2 iterations, 10 subsets, 192 × 192 matrix) and corrected for CT-based attenuation, dead time, random events, and scatter [20].

Statistical Analysis

Data was found to be indicated as mean ± standard error of the mean (SEM) and significance of comparison between the two data sets was determined through the use of SPSS 22.0 software (IBM Corp., Armonk, NY). Significance was defined as $P < 0.05$.

Results

Chemistry and Radiochemistry

The labeling precursors (P-FAPI and NOTA-FAPI-42) and reference compounds (^{19}F-FAPI-42 and ^{19}F-P-FAP) were successfully prepared using high chemical purity (>95%) and identified through the use of mass spectrometry (Supplementary data).

^{18}F-labeled FAP tracers (^{18}F-FAPI-42 and ^{18}F-P-FAP) were successfully prepared in automated manner via Al^{18}F-chelation on the AllInOne module. The total synthesis time was 40 ± 2 min, starting from the end of [^{18}F]F^- transfer to the synthesis module, in order to obtain the final product. The non-decay corrected labeling yield for ^{18}F-P-FAPI was 32% ± 6% (n = 8) and the measured specific activity was 46–182 GBq/μmol (n = 8). The non-decay corrected radiochemical yield for ^{18}F-FAPI-42 was 28% ± 8% (n = 10), and the specific activity was found to be 52–200 GBq/μmol (n = 10). Based on the monograph of "^{18}F-2-fluoro-2-deoxy-D-glucose injection" in the Chinses Pharmacopoeia, the acceptance criteria for the ^{18}F-P-FAPI and ^{18}F-FAPI-42 are summarized in table 1.

In Vitro Evaluation

The partition coefficients (log P) demonstrated high hydrophilic properties for ^{18}F-P-FAPI and ^{18}F-FAPI-42 with values of -2.72 ± 0.07 and -2.43 ± 0.02, respectively, which is similar to the clinically used radiotracer ^{68}Ga-FAPI-04 (-2.63 ± 0.04).

Determinizing the *in vitro* stability in PBS and mouse serum at 37 °C for 2 h indicates high stability across both tracers. We did not observe any decomposition (radiochemical purity >95%) across both tracers using radio-performance liquid chromatography (radio-HPLC). The *in vivo* stability of ^{18}F-P-FAPI and ^{18}F-FAPI-42 was also tested from mice blood after different times p.i., respectively. The parent of ^{18}F-P-FAPI was greater than 95% within the tested time. Nevertheless, the parent of ^{18}F-FAPI-42 at 15, 30, and 60 min constituted 20%, 15%, and 12%, respectively.

The binding affinity of P-FAPI, NOTA-FAPI-42, and DOTA-FAPI-04 for FAP was determined using SPR imaging, the results of which are shown in Fig. 3a. The K_d values for P-FAPI and NOTA-FAPI-42 are 0.73×10^{-10} M and 0.11×10^{-10} M respectively, and comparable to that of DOTA-FAPI-04 (0.63×10^{-10} M). These results indicate that the three radiotracers have high affinity towards FAP.

The FAP-positive A549-FAP cells and FAP-negative A549 cells for cell studies were identified in Supplemental Fig. 1. The binding properties of ^{18}F-P-FAPI and ^{18}F-FAPI-42 to FAP were evaluated across different cell lines and cell lines transfected with human FAP (Fig. 3b-e). ^{18}F-P-FAPI and ^{18}F-FAPI-42 indicated high uptake in FAP-positive A549-FAP and 293T-FAP cell lines and were significantly blocked by adding DOTA-FAPI-04. Additionally, FAP-negative A549 and 293T cells did not show any significant uptake of both tracers, suggesting a high specificity of both these tracers. Time-dependent uptake of ^{18}F-P-FAPI demonstrated a fast cellular uptake (>14 ID%/1 mio cells after 5 min; Fig. 3c) with a linear increasing uptake which reached a maximum of 66.4 ± 2.3 ID%/1 mio cells at 120 min, and can be significantly blocked by the adding DOTA-FAPI-04 to less than 0.8 ID%/1 mio cells. Internalization assays in A549-FAP cells demonstrates a rapid and high uptake of ^{18}F-P-FAPI and ^{18}F-FAPI-42 after 10 min of incubation with 76% and 65% internalized, respectively. Efflux experiments demonstrated that ^{18}F-P-FAPI exhibits a lack of significant cellular efflux in A549-FAP cells, which shows more than 95% of retention of the originally accumulated radioactivity during the 2 h incubation time. Efflux of ^{18}F-FAPI-42 from A549-FAP cells was almost linear during the 2 h incubation time. After the 2 h incubation, approximately 75% of the radioactivity was released from tumor cells.

MicroPET/CT and Biodistribution Studies

The dynamic microPET studies on mice bearing xenografts from human FAP-positive tumor cells were conducted using ^{18}F-P-FAPI. These results are represented through coronal microPET images taken at different time points p.i. (Fig. 4a). The PET images and time-activity curves demonstrate a rapid and high initial A549-FAP tumor uptake, which remains a constant increase over the total scan time of 120 min (Fig. 4c).

A comparison of PET imaging of ^{18}F-P-FAPI, ^{18}F-FAPI-42, and ^{68}Ga-FAPI-04 was conducted through the use of FAP-positive A549-FAP xenografts (Fig. 4b). Maximum intensity projections (MIP) indicated clear visualization of A549-FAP tumors with three radiotracers. ^{18}F-P-FAPI and ^{18}F-FAPI-42 were observed as the predominant liver excretions, as indicated by nonspecific uptake in the gallbladder and intestines. In comparison, ^{68}Ga-FAPI-04 was found to be mainly excreted via the renal route. Dynamic measurements over the course of 60 min p.i. revealed that the tumor uptake of ^{18}F-P-FAPI was significantly higher compared to ^{18}F-FAPI-42 and ^{68}Ga-PSMA-11 ($p < 0.05$). Therefore, ^{18}F-P-FAPI has a significantly higher tumor-to-background tissue contrast compared to the other two probes. In addition to the uptake in the tumor, both ^{18}F-P-FAPI and ^{18}F-FAPI-42 observed high uptake in joints (knee and shoulder), with uptake values (in %ID/g) of 5.49 ± 0.25, and 4.07 ± 0.04, respectively, at 1 h p.i. However, ^{68}Ga-FAPI-04 accumulated within the joints to a lower extent (0.90 ± 0.07 %ID/g). The blocking study for the tested three tracers in mice bearing A549-FAP tumors indicated a remarkable decrease in uptake by tumors and joints, demonstrating the specificity of radiotracers to its target protein.

In order to further confirm microPET imaging quantification, we conducted biodistribution studies of ^{18}F-P-FAPI with and without DOTA-FAPI-04 as competitor after 1 h of injection (Fig. 5). High and specific

uptake of tracers was observed in the A549-FAP tumors. The uptake in FAP-positive organs, including tumor and bone, was significantly reduced via co-injection of an excess of DOTA-FAPI-04, indicating FAP-specific targeting.

PET/CT Imaging and Analysis

The patient with nasopharyngeal cancer tolerated the examination and did not report any subjective effects after injection of ^{18}F-P-FAPI. There were no drug-related adverse events or physiologic responses. In the patient, ^{18}F-P-FAPI PET/CT showed an intense uptake of radioactivity within the primary tumor (SUV_{max} of 14.1) and lymph node metastases (SUV_{max} of 13.7 and 8.6, respectively), which was similar to ^{18}F-FDG PET/CT (Fig. 6). The uptake of ^{18}F-P-FAPI within the kidneys and bladder indicated that the main excretion organ was the kidney. Aside from this, the submandibular glands, pancreas and parotid gland were clearly visible at 1 h p.i. The primary tumor lesion and lymph node metastases were clearly defined on the ^{18}F-P-FAPI PET/CT due to low physiologic uptake of ^{18}F-P-FAPI within the brain. This result clearly indicates that this method can be successfully translated into a clinical setting.

Discussion

The main goal of our study was to identify ^{18}F-labeled FAP tracers for cancer imaging. Here, we report the synthesis and preclinical characterization of ^{18}F-P-FAPI and ^{18}F-P-FAPI-42, as well as the direct comparison with ^{68}Ga-FAPI-04 with regards to target binding and microPET imaging profile. In addition, a first-in-man study was conducted using ^{18}F-P-FAPI.

McBride *et al.* developed direct radiolabeling of peptides and proteins through chelation with Al^{18}F [21]. Our previous work also demonstrated that radiolabeling of peptides through complexation of Al^{18}F by radiometal chelator NOTA (1,4,7-triazacyclononane-*N*,*N*′,*N*″-triacetic acid) leads to good labeling yield and automated production [22]. In order to take advantage of the Al^{18}F-labeling method, we designed precursors with NOTA chelator. NOTA-FAPI-42 was obtained by substituting the DOTA (1,4,7,10-tetraazacyclododecane-1,4,7,10-tetraacetic acid) motif of FAPI-04 by the NOTA motif. For alterations of lipophilicity, we introduced the PEG (polyethylene glycol) linker between the pharmacophore and NOTA motif to obtain P-FAPI. Interestingly, the binding affinity of NOTA-FAPI-42 was approximately six-fold higher than that of the known tracer DOTA-FAPI-04, while P-FAPI displayed a similar binding affinity to DOTA-FAPI-04.

Preparation of ^{18}F-P-FAPI and ^{18}F-FAPI-42 was efficient and convenient using an automated synthesis module that has high specific activities. Since the linkers effect, lipophilicity of ^{18}F-P-FAPI was lower than that of ^{18}F-FAPI-42. Meanwhile, stability studies did not find any degradation of ^{18}F-P-FAPI either *in vitro* or *in vivo*, whereas ^{18}F-FAPI-42 was found to be degraded *in vivo*. These results indicate that ^{18}F-P-FAPI is more stable than ^{18}F-FAPI-42 *in vivo*.

Cellular uptake studies through the use of FAP-positive and FAP-negative cells indicated that both tracers were rapidly internalized with specific binding to FAP (Fig. 3). In addition, the amount of internalized activity of ^{18}F-P-FAPI was higher than that ^{18}F-FAPI-42. Efflux experiments demonstrated that ^{18}F-P-FAPI was significantly slower compared to ^{18}F-FAPI-42.

The microPET imaging results demonstrated that ^{18}F-P-FAPI had significantly higher tumor uptake compared to the other two probes, while ^{18}F-FAPI-42 had comparable tumor uptake in comparison to ^{68}Ga-FAPI-04. Moreover, uptake of ^{18}F-P-FAPI in tumor was clearly visualized at 15 min p.i. and uptake in all non-target organs, with the exception of liver and intestine decline over time, which leads to constant improvement in the tumor-to-background ratios. In addition, PET images from ^{18}F-P-FAPI and ^{18}F-FAPI-42 were observed through PET signals in the knee and shoulder joints, which is consistent with literature reported for ^{18}F-FGlc-FAPI in the mouse model. Therefore, the ^{18}F-labeled FAP tracers could do better than ^{68}Ga-FAPI-04 for FAP-dependent bone tissue remodeling in diseases such as rheumatoid arthritis by PET. The *ex vivo* distribution studies are consistent with PET imaging data. ^{18}F-P-FAPI indicated highest uptake within the gall bladder, indicating excretion mainly through the hepatobiliary pathway. The *in vivo* blocking experiment demonstrated that co-injection of DOTA-FAPI-04 significantly diminishes the tumor and joints uptake of the three tracers, and indicates high specificity of these tracers.

Based on above preclinical studies, we conducted the pilot clinical study of ^{18}F-P-FAPI in one nasopharyngeal cancer patient in order to examine the potential clinical application of FAP imaging. There were no subjective effects reported by the patient post-injection (p.i.) with a tracer. The pilot study provides tumor detectability of ^{18}F-P-FAPI in nasopharyngeal cancer. Fortunately, excretion of ^{18}F-P-FAPI in human predominant renal elimination is different from mice through the hepatobiliary pathway. Although limited by the numbers of patients available, our pilot study of ^{18}F-P-FAPI demonstrated promising imaging properties for cancer associated fibroblasts imaging. Furthermore, a study directly comparing ^{18}F-labeled FAP tracer versus ^{68}Ga-FAPI-04 in tumor patients is underway.

Conclusion

We developed a fluorine-18 labeled FAP-targeting tracers through automated preparation for imaging of cancer associated fibroblasts. The preclinical and primary clinical studies have demonstrated the safety and feasibility of ^{18}F-P-FAPI for further clinical translation, and successful imaging of nasopharyngeal cancer patient indicates potential values of ^{18}F-P-FAPI with regards to diagnosis, staging, and prognosis.

Declarations

Authors' contribution Study conception and design, Kongzhen Hu and Ganghua Tang; acquiring data, Kongzhen Hu, Yong Huang, Junqi Li, Li Li, Shimin Ye, and Yanjiang Han; analysis and interpretation of data, Kongzhen Hu, Lijuan Wang, Yong Huang, Junqi Li, and Jin Su; diagnostic imaging, Lijuan Wang and

Hubing Wu; data management, Shun Huang; drafting the manuscript, Kongzhen Hu; Revising the manuscript, Ganghua Tang and Jin Su. All authors read and approved the final manuscript.

Funding This work is supported by the National Natural Science Foundation of China (91949121 and 81701729), Outstanding Youths Development Scheme of Nanfang Hospital, Southern Medical University (2017J010), Nanfang Hospital Talent Introduction Fundation of Southern Medical University (123456), and Medical Scientific Research Foundation of Guangdong Province of China (A2019389) is gratefully acknowledged.

Declarations

Conflict of interests All authors declare no potential conflicts of interest.

Ethics approval This study was approved by the Ethics Committee of Nangfang Hospital (No. NFEC-2020-205 of October 01, 2020) and by the competent authorities and was conducted according to the latest guidelines of the Declaration of Helsinki. All animal studies were carried out and granted approval according to the guidelines of the Institutional Animal Care and Use Committee of Nanfang Hospital of Southern Medical University.
Statement of informed consent All patients gave written informed consent.

Competing interests

The authors declare that they have no competing interests.

References

1. Busek P, Mateu R, Zubal M, Kotackova L, Sedo A. Targeting Fibroblast activation protein in cancer - Prospects and caveats. Front. Biosci. - Landmark. 2018;23:1933–68.
2. Tran E, Chinnasamy D, Yu Z, Morgan RA, Lee CCR, Restifo NP, et al. Immune targeting of fibroblast activation protein triggers recognition of multipotent bone marrow stromal cells and cachexia. J. Exp. Med. 2013;210:1065–8.
3. Scanlan MJ, Raj BKM, Calvo B, Garin-Chesa P, Sanz-Moncasi MP, Healey JH, et al. Molecular cloning of fibroblast activation protein α, a member of the serine protease family selectively expressed in stromal fibroblasts of epithelial cancers. Proc. Natl. Acad. Sci. U. S. A. 1994;91:5657–61.
4. Šimková A, Bušek P, Šedo A, Konvalinka J. Molecular recognition of fibroblast activation protein for diagnostic and therapeutic applications. Biochim. Biophys. Acta - Proteins Proteomics [Internet]. Elsevier; 2020;1868:140409. Available from: https://doi.org/10.1016/j.bbapap.2020.140409
5. Liu F, Qi L, Liu B, Liu J, Zhang H, Che DH, et al. Fibroblast activation protein overexpression and clinical implications in solid tumors: A meta-analysis. PLoS One. 2015;10:1–18.

6. Park H, Lee Y, Lee H, Kim JW, Hwang JH, Kim J, et al. The prognostic significance of cancer-associated fibroblasts in pancreatic ductal adenocarcinoma. Tumor Biol. 2017;39:1–9.
7. Loktev A, Lindner T, Mier W, Debus J, Altmann A, Jäger D, et al. A tumor-imaging method targeting cancer-associated fibroblasts. J. Nucl. Med. 2018;59:1423–9.
8. Loktev A, Lindner T, Burger EM, Altmann A, Giesel F, Kratochwil C, et al. Development of fibroblast activation protein-targeted radiotracers with improved tumor retention. J. Nucl. Med. 2019;60:1421–9.
9. Giesel FL, Adeberg S, Syed M, Lindner T, Jiménez-Franco LD, Mavriopoulou E, et al. FAPI-74 PET/CT Using Either ^{18}F-AlF or Cold-Kit ^{68}Ga Labeling: Biodistribution, Radiation Dosimetry, and Tumor Delineation in Lung Cancer Patients. J. Nucl. Med. 2021;62:201–7.
10. Meyer C, Dahlbom M, Lindner T, Vauclin S, Mona C, Slavik R, et al. Radiation Dosimetry and Biodistribution of ^{68}Ga-FAPI-46 PET Imaging in Cancer Patients. J. Nucl. Med. 2020;61:1171–7.
11. Toms J, Kogler J, Maschauer S, Daniel C, Schmidkonz C, Kuwert T, et al. Targeting Fibroblast Activation Protein: Radiosynthesis and Preclinical Evaluation of an ^{18}F-Labeled FAP Inhibitor. J. Nucl. Med. 2020;61:1806–13.
12. Lindner T, Loktev A, Altmann A, Giesel F, Kratochwil C, Debus J, et al. Development of quinoline-based theranostic ligands for the targeting of fibroblast activation protein. J. Nucl. Med. 2018;59:1415–22.
13. Hintz HM, Gallant JP, Vander Griend DJ, Coleman IM, Nelson PS, LeBeau AM. Imaging Fibroblast Activation Protein Alpha Improves Diagnosis of Metastatic Prostate Cancer with Positron Emission Tomography. Clin. Cancer Res. 2020;26:4882–91.
14. Windisch P, Röhrich M, Regnery S, Tonndorf-Martini E, Held T, Lang K, et al. Fibroblast Activation Protein (FAP) specific PET for advanced target volume delineation in glioblastoma. Radiother. Oncol. [Internet]. The Author(s); 2020;150:159–63. Available from: https://doi.org/10.1016/j.radonc.2020.06.040
15. Shi X, Xing H, Yang X, Li F, Yao S, Zhang H, et al. Fibroblast imaging of hepatic carcinoma with ^{68}Ga-FAPI-04 PET/CT: a pilot study in patients with suspected hepatic nodules. Eur. J. Nucl. Med. Mol. Imaging. European Journal of Nuclear Medicine and Molecular Imaging; 2020;
16. Kratochwil C, Flechsig P, Lindner T, Abderrahim L, Altmann A, Mier W, et al. ^{68}Ga-FAPI PET/CT: Tracer uptake in 28 different kinds of cancer. J. Nucl. Med. 2019;60:801–5.
17. Tshibangu T, Cawthorne C, Serdons K, Pauwels E, Gsell W, Bormans G, et al. Automated GMP compliant production of [^{18}F]AlF-NOTA-octreotide. EJNMMI Radiopharm. Chem. EJNMMI Radiopharmacy and Chemistry; 2020;5:1–23.
18. Zhao S, Zhang B, Yang M, Zhu J, Li H. Systematic Profiling of Histone Readers in Arabidopsis thaliana. Cell Rep. [Internet]. ElsevierCompany.; 2018;22:1090–102. Available from: https://doi.org/10.1016/j.celrep.2017.12.099
19. Huang S, Li H, Han Y, Fu L, Ren Y, Zhang Y, et al. Synthesis and Evaluation of ^{18}F-Labeled Peptide for Gonadotropin-Releasing Hormone Receptor Imaging. Contrast Media Mol. Imaging. Hindawi;

2019;2019.

20. Tan H, Sui X, Yin H, Yu H, Gu Y, Chen S, et al. Total-body PET/CT using half-dose FDG and compared with conventional PET/CT using full-dose FDG in lung cancer. Eur. J. Nucl. Med. Mol. Imaging. European Journal of Nuclear Medicine and Molecular Imaging; 2020;
21. McBride WJ, Sharkey RM, Karacay H, D'Souza CA, Rossi EA, Laverman P, et al. A novel method of ^{18}F radiolabeling for PET. J. Nucl. Med. Society of Nuclear Medicine; 2009;50:991–8.
22. Huang S, Wu H, Li B, Fu L, Sun P, Wang M, et al. Automated radiosynthesis and preclinical evaluation of Al[^{18}F]F-NOTA-P-GnRH for PET imaging of GnRH receptor-positive tumors. Nucl. Med. Biol. [Internet]. Elsevier Inc.; 2020;82–83:64–71. Available from: https://doi.org/10.1016/j.nucmedbio.2020.02.004

Tables

Table 1 Tests items, acceptance criteria and test methods for ^{18}F-labeled FAP tracers

Test Items	Acceptance Criteria	Test Methods
Appearance	Colorless and particle-free	Visual inspection
pH	5.0–8.0	pH strip
Radiochemical purity a. [^{18}F]-labeled FAP tracers b. Sum [^{18}F]F^- and [^{18}F]AlF ≤5%	 ≥ 95% ≤ 5%	Radio-HPLC
Chemical purity Amount of AlF-precursor, precursor, and metal complexes of precursor Amount of sum of unidentified chemical impurities	 ≤ 5 μg/mL ≤ 5 μg/mL	HPLC with UV detector
Integrity of sterile filter membrane	Bubble point ≥ 1.5 bar	Bubble point determination
Residual solvent a. EtOH b. DMSO	 ≤ 10% v/v ≤ 0.1% v/v	GC
Total Radioactivity	50–5000 MBq/mL	Dose calibrator
Specific Activity	≥ 3GBq/μmol	HPLC with UV detector and Dose calibrator
Maximun injection volume	≤ 10 mL	Injector
Radionuclide identity-approximate half-life ($T_{1/2}$)	$T_{1/2}$ = 110 ± 5 min	Two time point radioactivity measurement in dose calibrator
Radionuclide identity – gamma spectrometry	Gamma energy is 0.511 ± 0.02 MeV, or a total peak 1.022 ± 0.02 MeV	Gamma spectrum on NaI (Tl) spectrometer
Radionuclide purity	≥ 99.8% of the activity of fluorine-18	Gamma spectrum on NaI (Tl) spectrometer
Sterility	No growth after 14 days of incubation at 37 °C	The Chinses Pharmacopoeia
Bacterial Endotoxins	≤17.5 EU per mL	*LAL Test* [a]

[a]Limulus amoebocyte lysate (LAL)

Figures

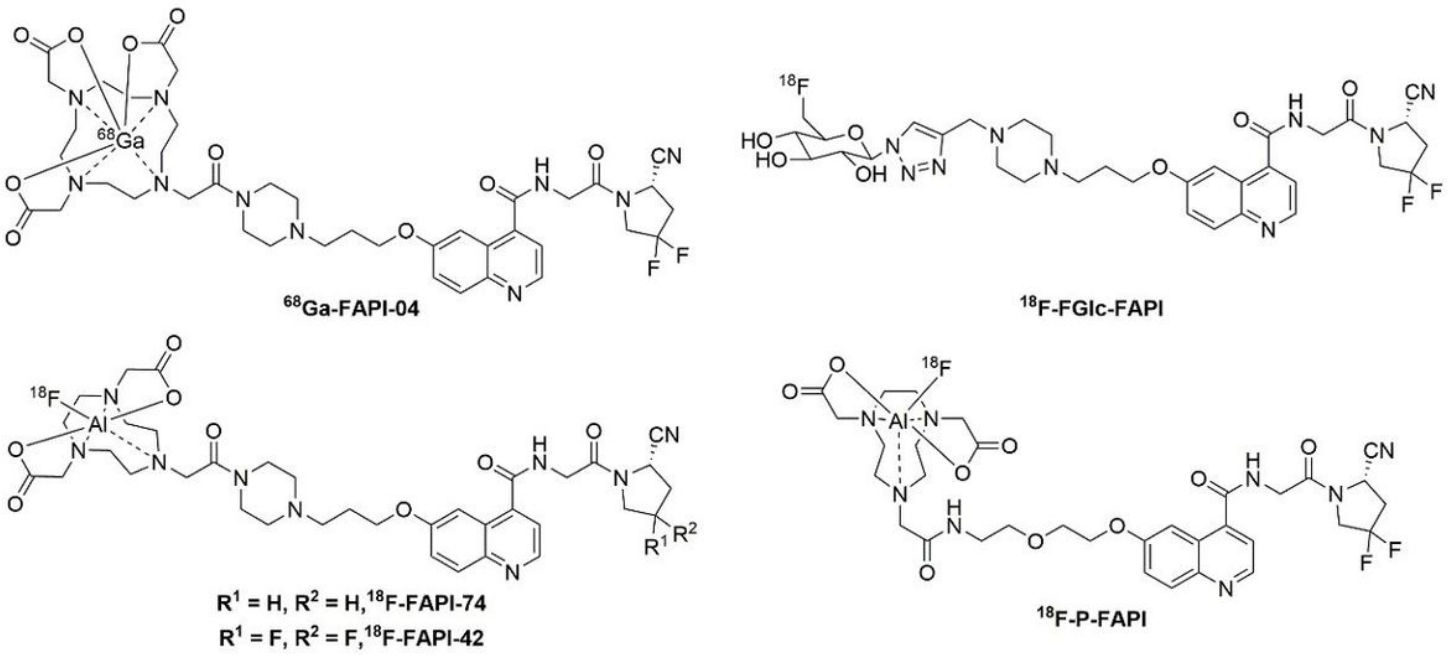

Figure 1

Structures of 68Ga-FAPI-04, 18F-FGlc-FAPI, 18F-FAPI-74, 18F-FAPI-42, and 18F-P-FAPI.

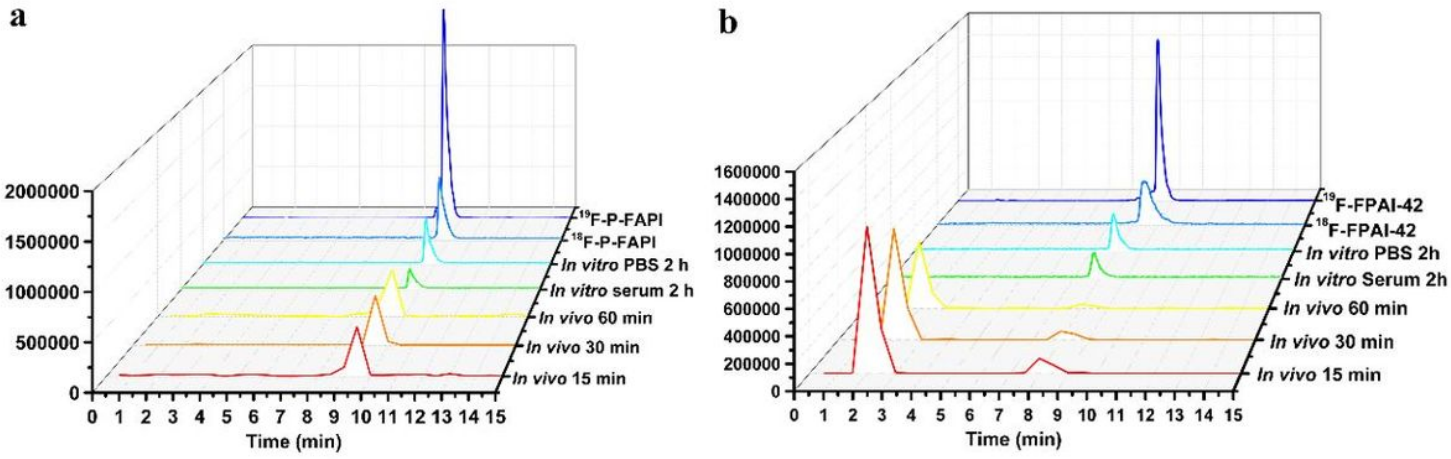

Figure 2

Identification and stability of 18F-P-FAPI and 18F-FAPI-42. Representative HPLC profiles for quality control, reference standard, in vitro stabilities, and in vivo metabolism studies of 18F-P-FAPI (a) and 18F-

FAPI-42 (b).

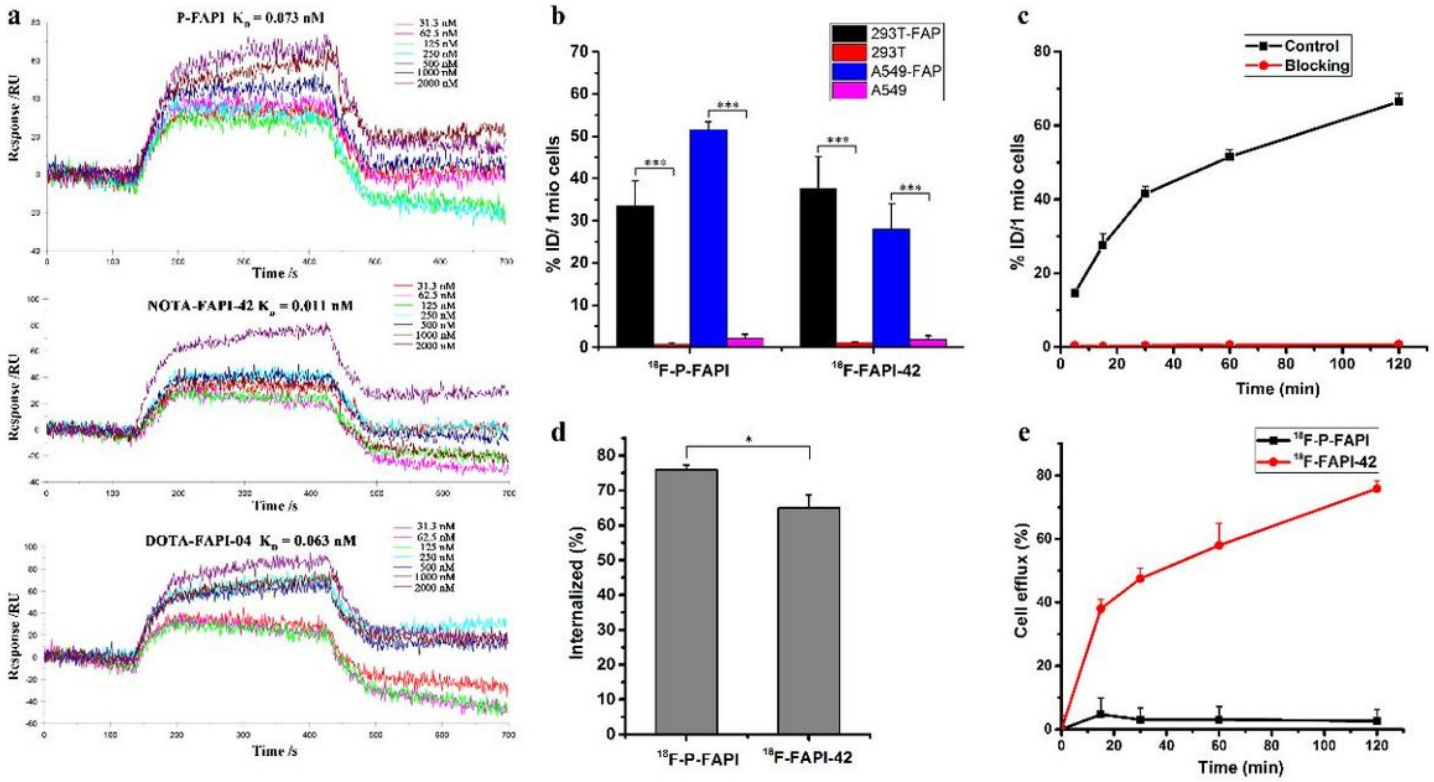

Figure 3

Binding affinity and cellular uptake. (a) The SPR assay determined binding kinetics constants (KD) between non-radioactive reference standards (P-FAP, NOTA-FAPI-42, and DOTA-FAPI-04) and human recombinant FAP proteins. (b) Binding of 18F-P-FAPI and 18F-FAPI-42 to different cell lines, including cell lines transfected with human FAP, after 60 min of incubation. (c) Uptake of 18F-P-FAPI in A549-FAP cells after incubation for 5 to 120 min, with and without blocking using DOTA-FAPI-04 as competitor. (d) Internalization of 18F-P-FAPI and 18F-FAPI-42 into A549-FAP cells after a 60 min incubation period. (e) Efflux kinetics of 18F-P-FAPI and 18F-FAPI-42 after 60 min incubation of A549-FAP cells with radiolabeled compounds, which was followed by incubation with compound-free medium for 5 to 120 min. The %ID/1 mio cells represents percentage of total applied dose normalized to 1 million cells. * $P < 0.05$; *** $P < 0.001$.

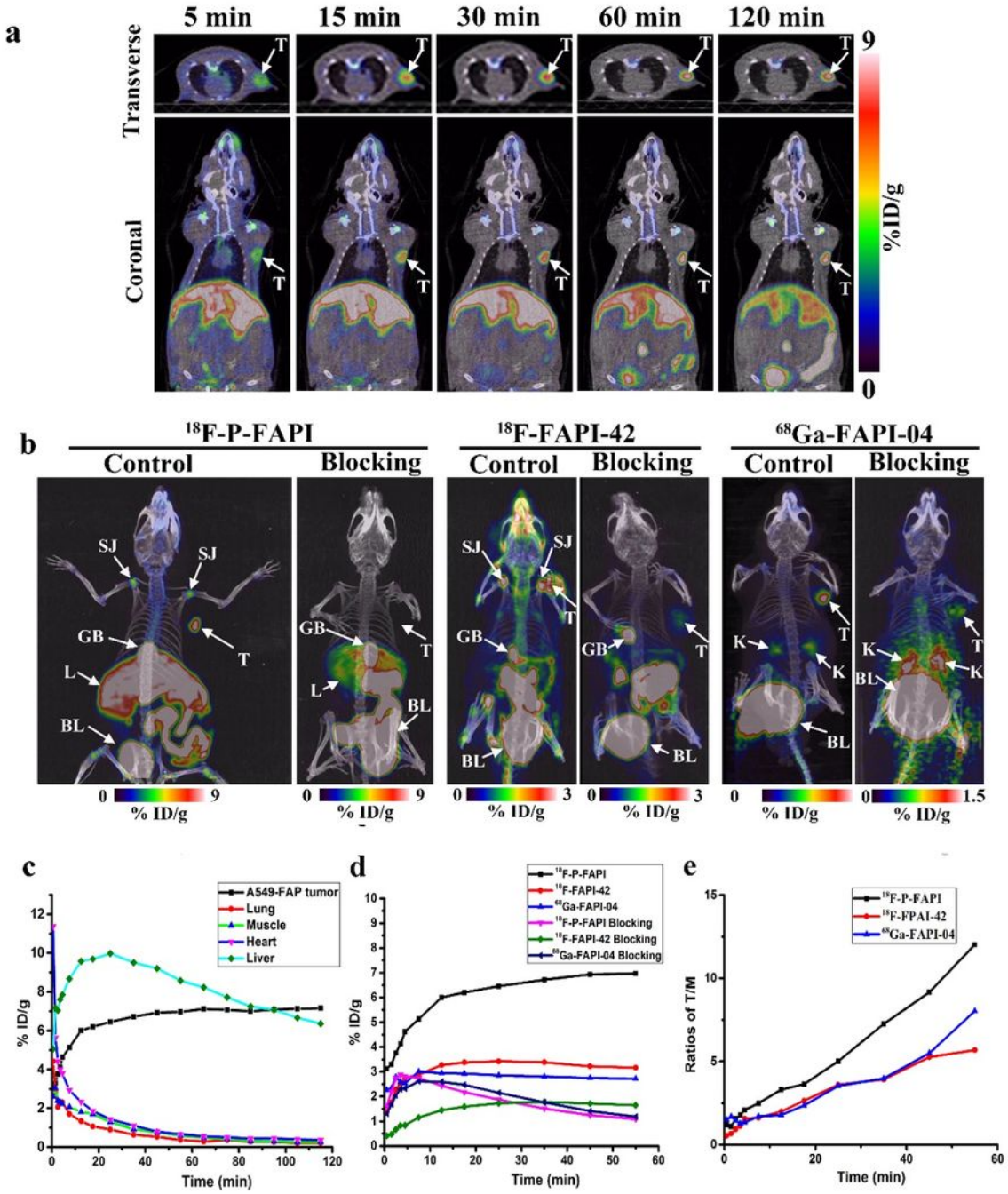

Figure 4

Representative microPET images and time-activity curves. (a) A series of coronal and transverse dynamic PET images of A549-FAP tumor bearing mice at 5, 15, 30, 60, 90, and 120 min p.i. of 18F-P-FAPI. The A549-FAP tumors are delineated in white arrows. (b) Maximum intensity projections (MIP) at 60 min post-intravenous injection of 18F-P-FAPI, 18F-FAPI-42, and 68Ga-FAPI-04 with and without DOTA-FAPI-04 as a competitor. Shoulder joint (SJ); tumor (T); gall bladder (GB); liver (L); bladder (BL). (c) Time-activity curves

of organs and A549-FAP tumor for 2 h p.i. of 18F-P-FAPI. (d) Time-activity curves of A549-FAP tumor uptake for 1 h after injection of 18F-P-FAPI, 18F-FAPI-42, and 68Ga-FAPI-04 with and without DOTA-FAPI-04 as a competitor. (e) The ratios of tumor-to-muscle for 1 h after injection of 18F-P-FAPI, 18F-FAPI-42, and 68Ga-FAPI-04, respectively.

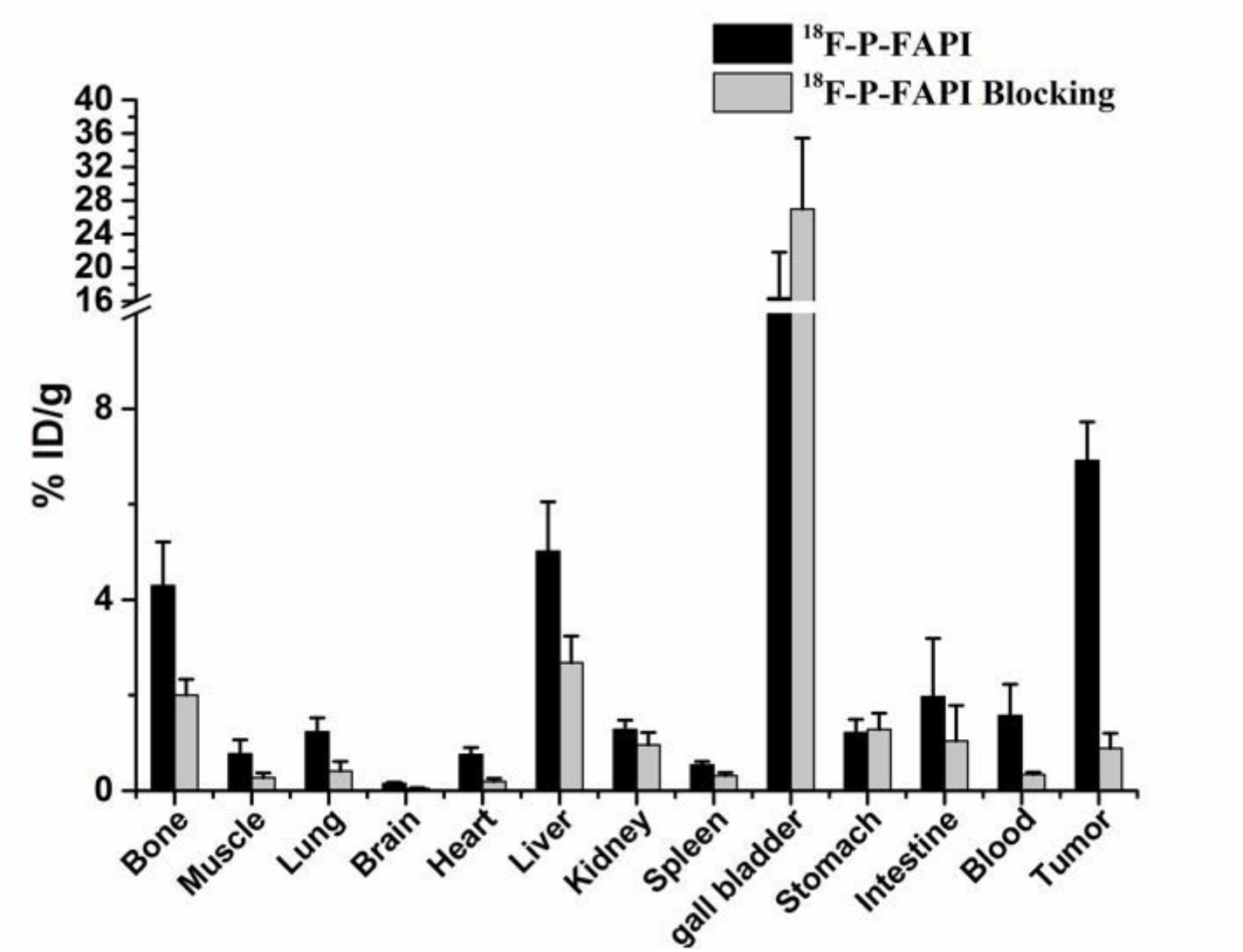

Figure 5

Biodistribution studies of 18F-P-FAPI in A549-FAP-bearing mice 1 h after intravenous injection. All data are expressed as mean value ± SD (n = 4).

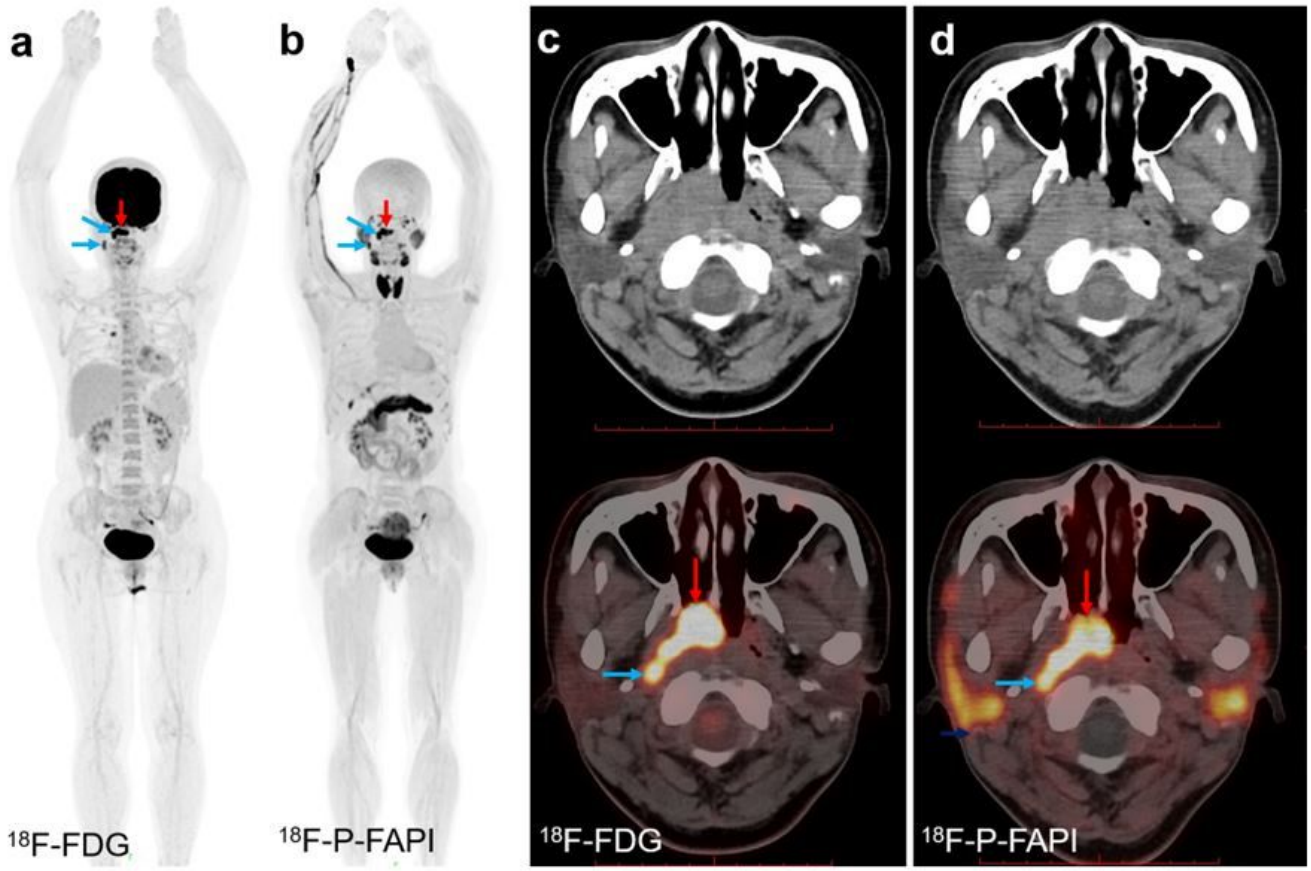

Figure 6

PET/CT images of a 41-year-old patient with newly diagnosed nasopharyngeal cancer. (a and c) The patient was examined using 18F-FDG in Sept 2020. (b and d) The second examination with 18F-P-FAPI was conducted 24 h later. 18F-P-FAPI images indicated tumor metastases uptake corresponding to 18F-FDG PET/CT images, represented by the arrow. Primary tumor is indicated by red arrows; lymph node metastases are indicated by blue arrows.

Supplementary Files

This is a list of supplementary files associated with this preprint. Click to download.

- Supportinginformation2021.2.21.docx
- Scheme1.tif